TENTH AUSTRALASIAN FLUID MECHANICS
CONFERENCE - UNIVERSITY OF MELBOURNE
11-15 DECEMBER 1989

SPATIAL RESOLUTION IN LASER BASED-SCALAR MEASUREMENTS

M.S. MANSOUR[1], R.W. BILGER[1] and R.W. DIBBLE[2]

[1]Department of Mechanical Engineering
The University of Sydney, NSW 2006, AUSTRALIA

[2]Combustion Research Facility
Scandia National Laboratories, Livermore, CA. , USA

Abstract

Spatial resolution effects in laser-based scalar measurements in turbulent flames is investigated. Scalar measurments in a reverse flow reactor (RFR) are made using a Raman/Rayleigh technique with two different probe volumes. In addition, estimates of the errors in the variance are investigated based on the scalar spectrum of Pao-Corrsin.

Predictions show that the errors depend on the sensor length relative to the integral and scalar length scales which are related by the turbulent Reynolds number. These predictions agree generally well with the experimental data. The data show that spatial averaging reduces any sharp peak of a monomodal *pdf* and reduces the peaks and fills in the gap in a bimodal distribution. Also, it reduces the variance and may change the mean.

INTRODUCTION

Laser-based measurement techniques have become a powerful tool for nonintrusive measurements in turbulent flames and flows with relatively small turbulence scales. With advanced laser diagnostics such techniques offer higher spatial-and-temporal resolution over traditional techniques. In turbulent combustion flows, velocity, species concentrations and temperature have been measured with great success by different laser techniques such as: Laser Doppler Velocimetery (LDV) (see Durst et al. 1981), Spontaneous Raman Scattering (SRS) (see Eckbreth 1988) and Rayleigh Scattering (RS) (see Dibble and Hollenbach, 1981).

Spatial-and-temporal resolution is usually assumed to be high enough, so that problems regarding this matter have been ignored. This assumption is often based on comparison between the length of the probe and the Kolmogorov length scale, L_K. It is often argued that significant contribution to turbulent fluctuations occurs only at probe lengths $> 10L_K$. Typically measurements are made in flows with a Kolmogorov length scale of 0.1 mm and a velocity of 50 m/s, using a probe of length 1 mm and laser pulse interval of 3 μs which allowing convection through 0.15 mm. The probe cannot spatially resolve flow quantities with turbulence scales smaller than the probe volume dimensions. In many cases the turbulence Reynolds number in flames is low and the probe is commensurate with the integral scales of the turbulence, so that errors in measured statistics may be significant.

Although great contributions have been made by these laser measurements in most aspects of turbulent combustion studies, the problem of spatial averaging effects has not yet been quantified.

Here, estimates of the spatial averaging effects on the measured variance are made based on the scalar spectrum for isotropic turbulence, giving results for a wide range of turbulent Reynolds numbers. These are compared with experimental data. The experimental data are based on scalar measurements of the species concentration and temperature by the Raman/Rayleigh technique at Sandia National Laboratories, Livermore, California (see Dibble et al. 1987) with two different probe volumes. The errors associated with these measurements due to spatial averaging on the mean, *rms* and on the shape of the *pdf* are presented and discussed. The data presented are for the species number densities of N_2 and H_2O and for Rayleigh signal which is the basis for temperature measurements. The information provided should prove useful in the application of laser-based measurements in turbulent flows.

ANALYTICAL ESTIMATES OF THE ERRORS

A. Errors in the Mean: The scalar quantity, Θ, such as temperature or species concentration, may be represented by its ensemble mean, $\overline{\Theta}$, and fluctuation from this mean, θ, where $\Theta = \overline{\Theta} + \theta$. The measured ensemble average, $\overline{\tilde{\Theta}}(\underline{x})$, in three dimensions, incorporating spatial averaging effects, can be derived (see Mansour et al. 1989a) as:

$$\overline{\tilde{\Theta}}(\underline{x}) = \int\int\int_{-\infty}^{\infty} \overline{\Theta}(\underline{x}+\underline{s}) h(\underline{s})\, ds_1 ds_2 ds_3 \,. \qquad (1)$$

where, h($\underline{s}$) is normalized measurements response function. Hence the error in the mean can be obtained by assessing the effect of the response function on the mean distribution. It will depend on the size of the measurement probe volume relative to the spatial variation in the mean field. In an axisymmetric mean field spatial averaging effects are minimized if the measurement length is aligned tangent to the mean scalar contours. Some errors remain due to variation along the finite length of the probe which is a chord in the circular distribution patterns. So,

$$\overline{\Theta}(x+s,y) = \overline{\Theta}(x,y) + R[(1+(\tfrac{s}{R})^2)^{1/2} - 1](\tfrac{d\overline{\Theta}}{dr})_R + \tfrac{1}{2}R^2[(1+(\tfrac{s}{R})^2)^{1/2} - 1](\tfrac{d^2\overline{\Theta}}{dr^2})_R + \ldots \qquad (2)$$

From using Eq. 2 in 1, with $\hat{r} = r/R$, we get:

$$\overline{\tilde{\Theta}}(x,y) = \overline{\Theta}(x,y) + C_{e_1}(\frac{d\overline{\Theta}}{d\hat{r}})_R + C_{e_2}(\frac{d^2\overline{\Theta}}{d\hat{r}^2})_R \qquad (3)$$

where, C_{e_1} and C_{e_2} may be called the first and second order error coefficients respectively, which are given for small $(l/2R)$, with l the probe length and R its radial location, by:

$$C_{e_1} = \frac{1}{6}(\frac{l}{2R})^2 - \frac{1}{40}(\frac{l}{2R})^4 \,,$$

$$C_{e_2} = \frac{1}{40}(\frac{l}{2R})^4 \,.$$

These coefficients are calculated for the present measurements to be in the order of 10^{-5} and 10^{-9} respectively, showing that the errors are mainly dominated by the first order gradient. However, these errors are estimated to be $< 1\%$ in the present investigation for most of the species and Rayleigh signal.

B. Errors in the Variance: The error in the measured variance may be obtained from analysis of the scalar

[1]Author to whom correspondence should be sent
[2]Combustion Research Facility, Sandia National Laboratories, Livermore, CA. USA

spectrum. The relationship between the true variance, $< \theta^2 >$, and one-dimensional scalar spectrum, $\psi(k_1)$, is

$$< \theta^2 > = \int_0^\infty \psi(k_1)\, dk_1 \,, \qquad (4)$$

with k_1 the wave number in the 1-component direction. The one-dimensional scalar spectrum is obtained from the three-dimensional spectrum, $F(k)$, for isotropic turbulence (see Hinze 1975) as:

$$\psi(k_1) = \int_{k_1}^\infty F(k)/k dk. \qquad (5)$$

The problem of a reacting mixture with non-isotropic turbulence is rather complicated. For simplicity, estimates are made for a nonreacting mixture with isotropic turbulence. Accordingly, the spectrum used here is that given by Corrsin (1964) and Pao (1964,1965) for the dissipative and inertial subranges:

$$F(k) = n\chi\epsilon^{-1/3}k^{-5/3}exp[-\frac{3}{2}nD\epsilon^{-1/3}k^{4/3}] \qquad (6)$$

where k is the wave number, n a universal constant taken as 0.59 (Gibson and Schwarz 1963),χ the molecular dissipation rate of the scalar variance, ϵ the dissipation rate of turbulent kinetic energy, and D the thermal diffusivity. In an early study by Wyngaard (1968, 1971) the probe length effect on the measured one-dimensional scalar spectrum was established. If the probe volume is set with the long dimension lying in the k_1 direction, the relation between the true and measured scalar spectrum is given by (Wyngaard, 1971):

$$\psi^m(k_1) = [sin^2(k_1.\frac{1}{2}l)/(k_1.\frac{1}{2}l)^2]\psi(k_1) \qquad (7)$$

The scalar rate of dissipation, χ, may be modelled as:

$$\overline{\chi} = R_s(\frac{\epsilon}{k_T}) < \theta^2 > = R_s(\frac{\epsilon^{1/3}}{L_I{}^{2/3}}) < \theta^2 > \qquad (8)$$

where R_s is the time scale ratio of the turbulence kinetic energy dissipation to the scalar dissipation, which can be taken (Beguier et al. 1978) to be 2, L_I is the integral length scale, and k_T is the turbulent kinetic energy. For $l << L_I$ most of the contribution due to spatial averaging on the measured scalar spectrum comes from the inertial and viscous subranges, so that the error in the variance can be estimated as:

$$\frac{< \theta^2 >^m}{< \theta^2 >} = 1 - nR_s \int_{\hat{k}_l}^\infty \int_{\hat{k}_1}^\infty \hat{k}_I^{2/3}\hat{k}_1^{-8/3} [1 - \frac{sin^2(\frac{\hat{k}_1}{2})}{(\frac{\hat{k}_1}{2})^2}]\, exp[-\tfrac{3}{2}n(\tfrac{L_\theta}{l})^{4/3}\hat{k}^{4/3}]d\hat{k}d\hat{k}_1 \qquad (9)$$

where $\hat{k}_I = l/L_I$; $\hat{k}_1 = l \times k_1$; $\hat{k} = l \times k$, with k as the wave number; and L_θ is the scalar microscale. The scalar microscale is related to the Kolmogorov length scale, L_K, as $L_\theta = Pr^{-3/4}L_K$, with Pr the Prandtl number and $L_K \equiv (\nu^3/\epsilon)^{1/4} \approx L_I/R_{e_t}{}^{3/4}$, with ν the kinematic viscosity and R_{e_t} the turbulent Reynolds number. Therefore, the errors in the measured variance depend on the length of the probe realtive to both the integral length scale, L_I, and the scalar microscale, L_θ, which are related by the turbulent Reynolds number and Prandtl number. The above equation can be solved numerically and the results are illustrated in Figure 1 for $Pr = 0.7$. The solid lines represent high turbulent Reynolds number, $Re_t > 500$, where the theory is expected to be valid while the dotted lines represent low turbulent Reynolds number, $Re_t < 500$. The error increases as R_{e_t} decreases for a constant l/L_θ (i.e. as l/L_I increases) while it decreases as R_{e_t} decreases for a constant l/L_I (i.e. as l/L_θ decreases). In Wyngaard's studies (1969, 1971) the length of sensors for χ and ϵ are only related to the scalar microscale and Kolmogorov length scale respectively: the χ sensor should not be longer than $2L_\theta$ and ϵ sensor no longer than $4L_k$ for a 10% error in χ and ϵ respectively.

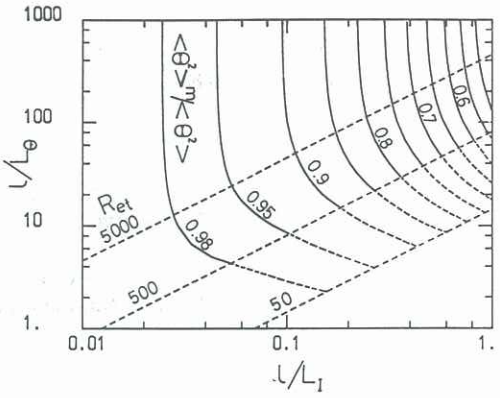

Fig. 1 Scalar variance response with the sensor length.

EXPERIMENTAL

The measurements have been conducted in a reverse flow reactor (RFR). Details of the reactor design and its design parameters and characteristics can be found in Ref. (Mansour et al. 1989b). The measurements have been carried out at two shear layers in the flame.

Simultaneous time-and-space resolved measurements of the species concentrations of CO_2, O_2, CO, N_2, CH_4, H_2O and H_2 and temperature are made by a Raman/Rayleigh technique, which is fully described by Dibble et al. (1987). The laser pulse is 3 μs time interval with beam width of 0.5 mm. The length of the probe volume, l, is varied between 1 mm to 1/3 mm. Variation of the length of the probe is made by changing the inlet slit, which collects the Raman and Rayleigh scattered light at 3 × magnification factor. So, the corresponding inlet slit width is 3 mm and 1 mm, denoted as slit settings S3 and S1 respectively.

RESULTS AND DISCUSSION

The measurements have been carried out with two different probe volumes in a flame with 40 m/s mean exit jet velocity and 0.7 mean equivalence ratio at two shear layers. The data presented here are for the species number densities ($molecules/cm^3$) of N_2 and H_2O and a calibrated Rayleigh signal. Mean, rms fluctuation, higher moments (skewness and kurtosis) and probability density functions (pdfs) are used to illustrate these data. Compensating the effect of the errors in the mean and variance (as shown later) on the shape of the pdf can be made by plotting $(\Theta - \overline{\Theta})/\overline{\Theta'^2}^{1/2}$ versus $p(\Theta) \times \overline{\Theta'^2}^{1/2}$, where $p(\Theta)$ is the prbability of Θ. The data are represented in Figs. 2-5 for a calibrated Rayleigh signal, $\hat{R}_R$, (Figs. 2 and 3), and number densities of H_2O (Fig. 4) and N_2 (Fig. 5). The ensemble mean, rms fluctuations (standard deviation), coefficient of variation, C_{v_i}, moment coefficients of skewness and kurtosis are listed in these figures. The coefficient of variations, C_{v_i}, is defined as the standard deviation normalized by the mean value. The moment coefficients of skewness (a_3) and kurtosis (a_4) are defined as m_3/rms^3 and m_4/rms^4 respectively, with m_3 and m_4 the third and fourth central moments respectively. Spatial averaging effects on these coefficients (a_3 and a_4) are discussed later with the effects on the shape of the pdf.

From Figs. 2-5, the ensemble means of the scalar quantities measured with setting S3 are found to be in error relative to those with setting S1. The average error is $\sim 2\%$. The errors in the mean can be attributed in part to the standard error with random sampling and in part due to a possible change of the optical collection efficiency. The standard error due to random sampling, which is equal to the ratio of the rms fluctuations to square root of N, where N is the total number of samples, is estimated to be in the order of 0.7 % of the mean, with 5000 shots. Also, part

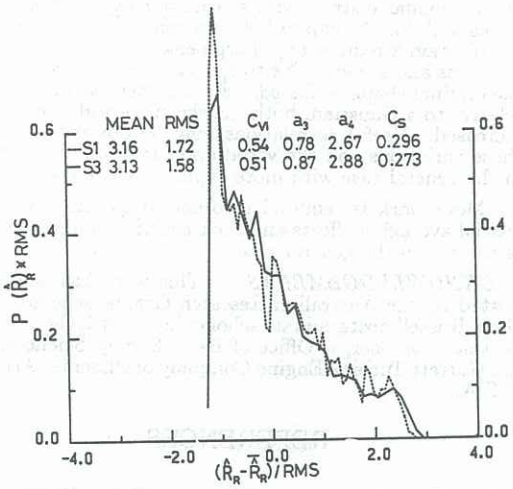

Fig. 2 Normalized single *pdf*s of the calibrated Rayleigh signal, $\hat{R}_R$, at the inner shear layer: continuous line for S3 and dotted line for S1.

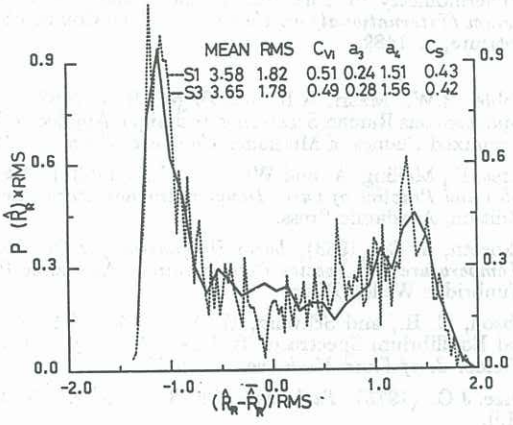

Fig. 3 Normalized single *pdf*s of the calibrated Rayleigh signal, $\hat{R}_R$, at the outer shear layer: continuous line for S3 and dotted line for S1.

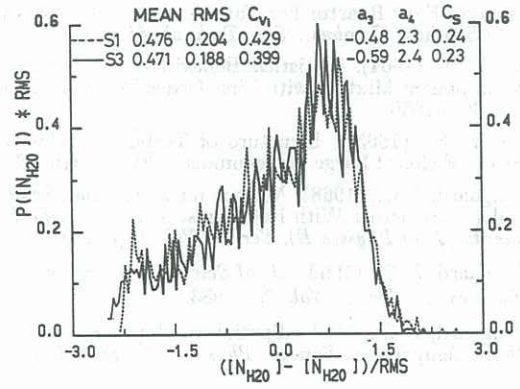

Fig. 4 Normalized single *pdf*s of the number density H_2O at the inner shear layer: continuous line for S3 and dotted line for S1.

of these errors may be attributed to the spatial averaging effects as estimated above. where the errors are estimated to be $< 1\%$ in the present investigation for most of the species and Rayleigh signal.

The errors in the measured variance can be attributed in part to its standard sampling error, which is approx-

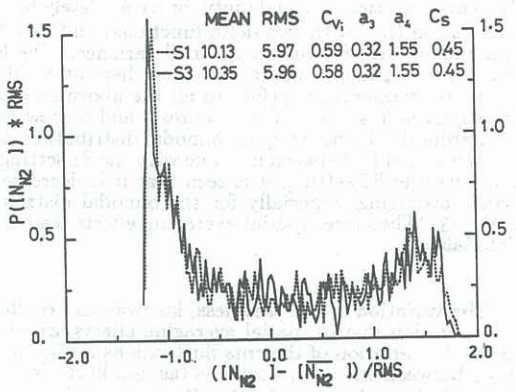

Fig. 5 Normalized single *pdf*s of the number density N_2 at the outer shear layer: continuous line for S3 and dotted line for S1.

imately equal to $(\frac{2}{N})^{1/2}$ of the variance (i.e. 2% of the variance for 5000 shots), while the major contribution is due to spatial averaging effects. These later errors are estimated above from scalar spectrum analysis. The errors in the mean are largely due to calibration errors, which also affects the variance. Hence, the coefficient of variation, C_{v_i}, is more appropriate to use in our comparison between the errors in the measurements and the estimated ones. The comparison is illustrated in Table 1, where $\Re_m$ and $\Re_p$ are the measured and predicted ratios of the coefficient of variation with S3 to that with S1 respectively. It shows that the predictions are slightly lower than the measurements. This can be attributed in part to the sampling errors and most likely to the assumptions made in the predictions. In general, however, the predictions are quite consistent with the measurements.

TABLE 1
Comparison between measured and predicted response of the coefficient of variation, C_{v_i}.

Species or $\hat{R}_R$	Flame Region	Pr	L_θ μm	$\Re_m$ %	$\Re_p$ %
N_2	inner layer	0.73	86	98.2	92.6
	outer layer	0.70	122	97.6	94.1
H_2O	inner layer	1.02	67	93.0	92.1
$\hat{R}_R$	inner layer	0.81	80	92.7	92.4
	outer layer	0.77	110	95.8	93.9

In the present measurements, spatial averaging effects are not large enough to change the overall shape of the *pdf* greatly, as shown in Figs. 2-5. However, within the range of the operating conditions here, some effects have been observed and can be discussed, based on the higher moments of the *pdf* (e.g. skewness and kurtosis), as:

1. For a monomodal distribution, as shown in Fig. 2, spatial averaging effects reduce the sharp peak, while in Fig. 4 no much effects can be detected. The moment coefficients of skewness, a_3, and kurtosis, a_4, are increased by spatial averaging. The kurtosis is less than 3 and increases towards 3 (i.e. towards Gaussian distribution) in all cases. The increase of a_4 towards Gaussian for $a_4 < 3$ may imply that spatial averaging shifts the shape of the *pdf* to Gaussian. This needs more data, especially with $a_4 > 3$, to be quantified.

2. For a bimodal distribution, as shown in Figs. 3 and 5, skewness, a_3, and kurtosis, a_4, are increased by spatial averaging. In Figure 3, spatial averaging effects reduces the peaks and fills the gap in between them, which we may say reduce its bimodality. In Figure 5 no effect can be detected on the shape of the *pdf* of nitorgen, which also shows equal skewness and kurtosis. A measure of bimodality can be made using a coefficient of segregation, C_s, (defined $C_s \equiv \overline{\Theta'^2}/(\Theta_2 - \overline{\Theta})(\overline{\Theta} - \Theta_1)$, where $\overline{\Theta}$, Θ_1 and Θ_2 are the mean, lower limit and upper limit of the range of

Θ). This coefficient is equal unity for a completely bimodal distribution (i.e. with two delta functions) and zero for a monomodal one of vanishingly small variance. The lower and upper limits Θ_1 and Θ_2 are taken here at a value of 5% of the maximum of $p(\Theta)$. In all the above mentioned figures, C_s is less than unity. Figures 3 and 5 show values of C_s around 0.4 where a quite bimodal distribution exists. Comparison of C_s between its value with the S1 setting and that with the S3 setting, it is seen that it is decreased by spatial averaging, especially for the bimodal distribution in Fig. 3. Therefore, spatial averaging effects lead to less bimodality.

The variation of the skewness, kurtosis and coefficient of segregation due to spatial averaging effects are plotted versus the variation of the *rms* fluctuations in Fig. 6. The ratios between the *rms*, skewness (as a_3), kurtosis (as a_4) and coefficient of segregation (as C_s) at S3 setting to those at S1 setting may be denoted as $R(s)$, $R(a_3)$, $R(a_4)$ and $R(C_s)$ respectively. The data illustrated in Fig. 6 represent those listed in Figs. 2-5. The data set may not be sufficient to give general trends. The variation of $R(a_3)$ and $R(a_4)$ relative to the the variation in $R(s)$ depends on the original shape of the *pdf*, which increase as $R(s)$ decrease for a distribution flatter than a Gaussian (i.e. $a_4 < 3$, as found here) and may decrease for a distribution peakier than a Gaussian.

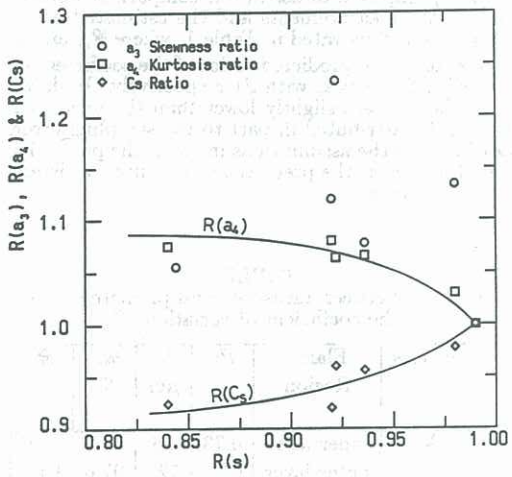

Fig. 6 Variation of the moment coefficients of skewness and kurtosis, $R(a_3)$ and $R(a_4)$, and the coefficient of segregation, $R(C_s)$, with the variation of the *rms*, $R(s)$, due to spatial averaging effects.

CONCLUSION

Spatial averaging effects on laser-based scalar measurements have been investigated experimentally and compared with estimates. Based on this investigation and comparisons the following conclusions can be made:

1. Predictions show that the errors in the measured variance depend on the integral and scalar length scales, which are related by the turbulent Reynolds number and Prandtl number. These errors which are estimated by Eq. 9 for isothermal, isotropic and nonreacting flow, show generally good agreement with the measurements in a reacting flow.

2. Spatial averaging reduces the variance, and may change the mean (for a non-linear profile of the mean within the probe volume). The errors are somewhat higher for the reactive scalars and Rayleigh signal relative to those for the non-reacting species.

3. The general shape of the *pdf* is not greatly affected by the spatial averaging in the present data. However, for a bimodal distribution, spatial averaging reduces the peaks and fills the gap in between, while for a monomodal distribution it reduces any sharp peak. The variation of the skewness and kurtosis due to spatial averaging depends on the original shape of the *pdf*. For a flatter *pdf* distribution relative to a Gaussian, both the skewness and kurtosis are increased. Useful correlations may be obtained between those variations and the variation of the *rms* fluctuations in the general case with more experimental data.

More work is required in order to quantify fully the spatial averaging effects and their contribution to the form of the *pdf* in the general case.

ACKNOWLEDGEMENTS This work has been supported by the Australian Research Grants Scheme, Peter Nicol Russell postgraduate scholarship award, the U.S. Department of Energy, Office of Basic Energy Sciences, and the Garrett Turbine Engine Company of Phoenix, Arizona, U S A.

REFERENCES

Beguier, C., Dekeyser, I. and Launder, B.E., (1978). *Phys. Fluids 21*, 307.

Corrsin, S., (1964). Further Generalization of Onsager's Cascade Model for Turbulent Spectra. *Phys. Fluids 7*, 1156.

Dibble, R. W., and Hollenbach, R. E., (1981). Laser Rayleigh Thermometry in Turbulent Flames. *Eighteenth Symposium (International) on Combustion*, The Combustion Institute, p. 1489.

Dibble, R.W., Masri, A.R. and Bilger, R.W. (1987). The Spontaneous Raman Scattering Technique Applied to Non-Premixed Flames of Methane. *Combust. Flame 67*, 189.

Durst, F., Melling, A. and Whitelaw, J.H., (1981). *"Principles and Practice of Laser Doppler Anemometery"*, Second Edition, Acadamic Press.

Eckbreth, A. C., (1988). *Laser Diagnostics for Combustion Temperature and Species Concentration.* Acadamic Press, Tunbridge Wells, UK.

Gibson, C. H., and Schwarz, W. H., (1963). The Universal Equilibrium Spectra of Turbulent Velocity and Scalar Fields. *J. of Fluid Mech. vol. 16*, p.365.

Hinze, J.O., (1975). *Turbulence*, Ch. 3, Second Ed., McGraw-Hill.

Mansour, M.S., Bilger, R.W. and Dibble, R.W. (1989b). Spatial Averaging Effects in Raman/Rayleigh Measurements in Turbulent Flames. *Combust. Flame* (submittd).

Mansour, M.S., Bilger, R.W. and Stårner, S. H., (1989a). A Reverse Flow Reactor For Turbulence/Chemistry Interaction Studies. *Combust. Sci. Technol. 65*, p.83.

Pao, Y. H., (1964). Statistical Behavior of a Turbulent Multicomponent Mixture with First-Order Reactions *AIAA J.* vol. 2, p.1550.

Pao, Y. H., (1965). Structure of Turbulent Velocity and Scalar Fields at Large Wavenumbers. *Phys. Fluids 8*, 1063.

Wyngaard, J. C., (1968). Measurements of Small-Scale Turbulence Structure With Hot Wires. *J. of Scientific Instruments (J. of Physics E), Ser. 2, Vol. 1*, p. 1105,

Wyngaard, J. C., (1969). *J. of Scientific Instruments (J. of Physics E), Ser. 2, Vol. 2*, p. 983.

Wyngaard, J. C., (1971). Spatial Resolution of a Resistence Wire Temperature Sensor. *Phys. Fluids 14*, 2052.